Accepted Manuscript

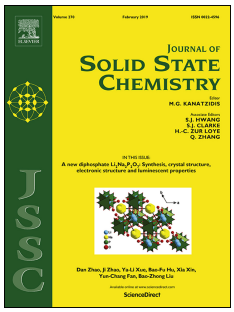

Effect of partial substitution of Ca for Sr on crystal structure and luminescence of Ce-doped $Sr_4Al_{14}O_{25}$

M. Misevicius, K. Jonikavicius, J.-E. Jørgensen, V. Balevicius

PII: S0022-4596(19)30136-7

DOI: https://doi.org/10.1016/j.jssc.2019.03.026

Reference: YJSSC 20675

To appear in: *Journal of Solid State Chemistry*

Received Date: 5 February 2019

Revised Date: 15 March 2019

Accepted Date: 15 March 2019

Please cite this article as: M. Misevicius, K. Jonikavicius, J.-E. Jørgensen, V. Balevicius, Effect of partial substitution of Ca for Sr on crystal structure and luminescence of Ce-doped $Sr_4Al_{14}O_{25}$, *Journal of Solid State Chemistry* (2019), doi: https://doi.org/10.1016/j.jssc.2019.03.026.

Effect of partial substitution of Ca for Sr on crystal structure and luminescence of Ce-doped $Sr_4Al_{14}O_{25}$

M. Misevicius, K. Jonikavicius, J.-E. Jørgensen, V. Balevicius

Table of contents:

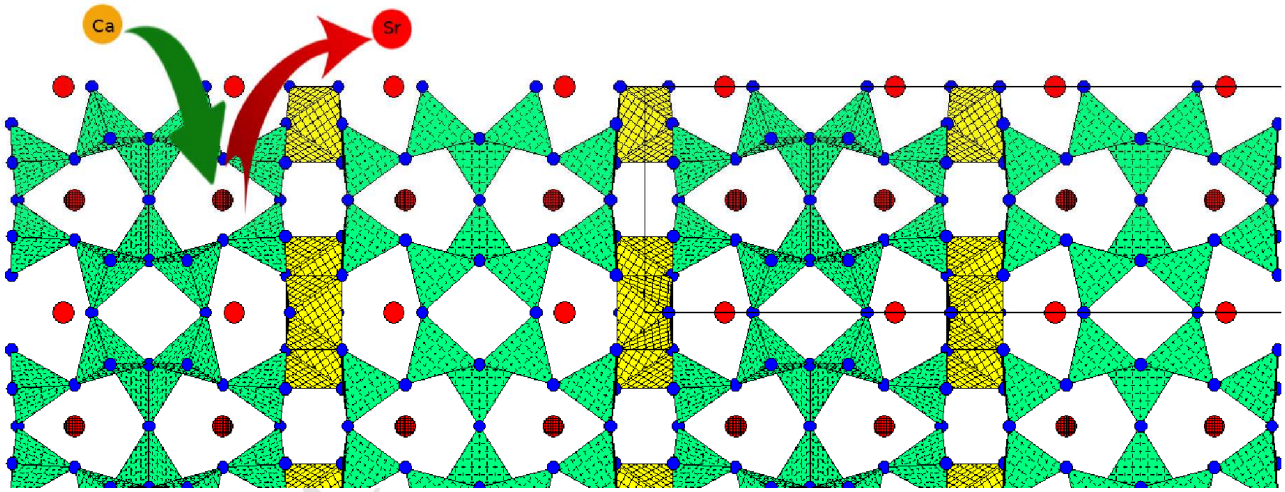

Effect of partial substitution of Ca for Sr on crystal structure and luminescence of Ce-doped $Sr_4Al_{14}O_{25}$

M. Misevicius[a,b,*], K. Jonikavicius[b,c], J.-E. Jørgensen[c], V. Balevicius[a]

[a]*Institute of Chemical Physics, Faculty of Physics, Vilnius University, Saulėtekio al. 3, LT-10257 Vilnius, Lithuania*

[b]*Institute of Chemistry, Faculty of Chemistry and Geosciences, Vilnius University, Naugarduko street 24, LT-03225 Vilnius, Lithuania*

[c]*Department of Chemistry, Aarhus University, DK-8000 Aarhus C, Denmark*

**Corresponding author, e-mail: martynas.misevicius@chf.vu.lt*

Abstract

Monophasic undoped and cerium-doped $Sr_4Al_{14}O_{25}$ samples with partial substitution of calcium for strontium were prepared using conventional solid-state synthesis. Structural studies revealed that substitution of strontium by calcium in $Sr_{4-x}Ca_xAl_{14}O_{25}$ up to x=1.4 is possible without formation of additional phases and that the Sr2 site (of two possible) is more likely to be substituted by the smaller Ca ions. Photoluminescence measurements of $Sr_4Al_{14}O_{25}$:Ce showed emission with double peak (360 and 380 nm) under 330 nm excitation wavelength. The effect of partial substitution of strontium by calcium on the luminescence of $Sr_{4-x}Ca_xAl_{14}O_{25}$:Ce (emission, quantum yield, decay) were studied as well.

Keywords: Oxides; crystal structure; optical properties; X-ray diffraction; luminescence.

1. Introduction

The discovery of advanced optical materials with multiple superior qualities for display applications remains a difficult problem. The specific luminescence properties of multinary oxides are highly sensitive to the changes in dopant composition, host stoichiometry, and processing conditions [1-4]. Inorganic luminescent materials in most cases consist of rear-earth ions embedded in a crystal matrix. Part of the widely studied matrices for luminescent materials is the group of strontium aluminates. In $SrO\text{-}Al_2O_3$ system, there are several well-known phases, namely $Sr_3Al_2O_6$, $SrAl_2O_4$, $SrAl_4O_7$, $SrAl_{12}O_{19}$, $Sr_4Al_2O_7$, $Sr_4Al_{14}O_{25}$, $Sr_{12}Al_{14}O_{33}$ and $Sr_{10}Al_6O_{19}$, as described in the literature [5]. Eu^{2+}-doped $SrAl_2O_4$ is one of the most studied systems in the family of strontium aluminates and it shows strong green emission at ~530 nm [6, 7].

However, during recent years, a great deal of attention has been paid to $Sr_4Al_{14}O_{25}$ phase [8-33]. The crystal structure of $Sr_4Al_{14}O_{25}$ has been determined to be orthorhombic with space group Pmma and a = 24.7451(2)Å, b = 8.4735(6)Å , c = 4.8808(1)Å, V = 1023.41(3) $Å^3$, Z = 2, and D=3.66 g/cm^3 [34]. Capron et al. showed that this phase forms at 1134 ˚C and is stable up to 1500 ˚C [35]. $Sr_4Al_{14}O_{25}$:Eu has been focused for white LEDs, because it has a greenish-blue emission band at 495 nm by nUV excitation and a quantum efficiency of 90% [36]. If co-doped with dysprosium, $Sr_4Al_{14}O_{25}$:Eu,Dy has been reported to show persistent luminescence with an afterglow of more than 20 h [8-11]. Other dopants have also been incorporated in this phase. Red luminescence has been observed in $Sr_4Al_{14}O_{25}$:Cr,Eu,Dy [12] and $Sr_4Al_{14}O_{25}$:Mn [13, 37]. Samarium doped compounds exhibited orange red emission [14, 15]. Blue green $Sr_4Al_{14}O_{25}$:Eu,Tm,La phosphor has also been reported [16]. Cerium-doped $Sr_4Al_{14}O_{25}$ phosphors have been studied previously, but the reported emission wavelengths are at 400 nm (λ_{ex} = 350 nm) [17], at 472 and 511 nm (λ_{ex} = 275 nm) [18] or at 314 nm (λ_{ex} = 262 nm) [19]. Such different results might be due to different synthesis methods used in researches, but still it shows that more investigation is required.

The effects of nonstoichiometry and cationic substitution on photoluminescence and afterglow characteristics of strontium aluminate phosphor ($Sr_4Al_{14}O_{25}$:Eu^{2+}, Dy^{3+}) has been investigated by Suriyamurthy and Panigrahi [30]. The authors reported that calcium-substituted samples show decreased photoluminescence intensities and in case of higher degree of substitution – blue shifts of emission spectra are visible. The photoluminescence emission intensity from barium-substituted samples was significantly enhanced compared with that of the unsubstituted one. A similar study has been carried out by Dacyl et al. [25], in which it is also reported that substitution by calcium resulted in a blue shift of the emission spectrum. On the other hand, both studies deal with samples that mostly consist of several phases. In the current study cerium was chosen as an activator since it is one of most promising activators in non-Eu^{2+}-based persistent luminescent materials [38]. In order to investigate the effects of strontium substitution by calcium on crystal structure of $Sr_4Al_{14}O_{25}$ and luminescent properties of related cerium-doped samples, single-phase materials were synthesized and subjected to detailed investigations in the present study.

2. Experimental

All $Sr_4Al_{14}O_{25}$, $Sr_{(4-x)}Al_{14}O_{25}Ce_x$ and $Sr_{(3.95-x)}$ $Al_{14}O_{25}Ce_{0.05}Ca_x$ samples were synthesized using conventional solid-state synthesis method. Stoichiometric amounts of strontium carbonate ($SrCO_3$, 97.5%, AlfaAesar), calcium carbonate ($CaCO_3$, 99%, CarlRoth) alumina (Al_2O_3, 99.5% NanoDur™, AlfaAesar) and cerium nitrate ($Ce(NO_3)_3 \cdot 6\ H_2O$, 99%, Merck) were mixed in an agate mortar. Also 2.5% by weight of H_3BO_3 (99.8 %, CarlRoth) was added as a fluxing agent. The starting mixtures were heated to 1300 □ using a heating rate of 5 °/min and held it for 10 h. In the case of cerium containing samples, the same heating approach was used, however, activated carbon powder was used to create a reducing atmosphere. In order to achieve this, smaller open crucible with the starting mixture was placed inside a larger crucible containing excess of activated carbon powder, which was closed with a lid.

Powder X-ray diffraction (XRD) measurements for initial phase analysis were performed using Rigaku MiniFlex II diffractometer working in Bragg-Brentano (Θ/2Θ) geometry. The data were collected at a step of 0.01º and at speed of 10 º/min using Cu Kα radiation. In order to obtain data for structural refinement, Rigaku SmartLab diffractometer was used working in a parallel beam (Θ/Θ) geometry, using 5.0º Soller slits and Cu $K\alpha_1$ (λ = 1.54059 Å) radiation. Samples were spun at 30 rpm, measurements were taken at a step of 0.01º and at speed of 4 º/min. Rietveld refinement in this work was performed using *FullProf* software[39].

Quantum yield, excitation and emission spectra were recorded using Edinburgh Instruments FLS980 spectrometer equipped with double excitation and emission monochromators, 450 W Xe arc lamp, a cooled (–20 °C) single-photon counting photomultiplier (Hamamatsu R928) and mirror optics for powder samples. The excitation spectra were corrected by a reference detector. In both cases step width was 0.5 nm and integration time was 0.4 s. Quantum yields (QY) were calculated by measuring emission spectrum of the sample in Teflon coated integration sphere. The values were obtained by employing the following equation:

$$QY = \frac{\int I_{em,sample} - \int I_{em,Teflon}}{\int I_{ref,Teflon} - \int I_{ref,sample}} \times 100\%$$

where $\int I_{em,sample}$ and $\int I_{em,Teflon}$ are integrated emission intensities of the sample and Teflon, respectively; $\int I_{ref,sample}$ and $\int I_{ref,Teflon}$ are the integrated reflectance of the sample and Teflon, respectively [40]. The photoluminescence decay kinetics studies were performed on the same FLS980 spectrometer. Decay curves were fitted using monoexponential decay function: $I(t)=I_0\, e^{-t/\tau}$, where τ is decay constant, $I(t)$ – intensity at a given time, I_0 – initial intensity and t – time.

3. Results and discussion

3.1. Synthesis of monophasic $Sr_4Al_{14}O_{25}$

The $Sr_4Al_{14}O_{25}$ samples prepared using boric acid as a fluxing agent (2.5 wt.%) were single phase compounds. Results of Rietveld refinement are shown in Figure 1. The original crystallographic data of Wang et al. [34] were used as a starting model for Rietveld refinement of X-ray diffraction data collected at room temperature. The refinement smoothly converged to the structure close to the starting model based on X-ray powder diffraction data. Therefore, it was determined that $Sr_4Al_{14}O_{25}$ phase can be synthesized by heating at 1300 °C for 8 h using the solid state reaction method.

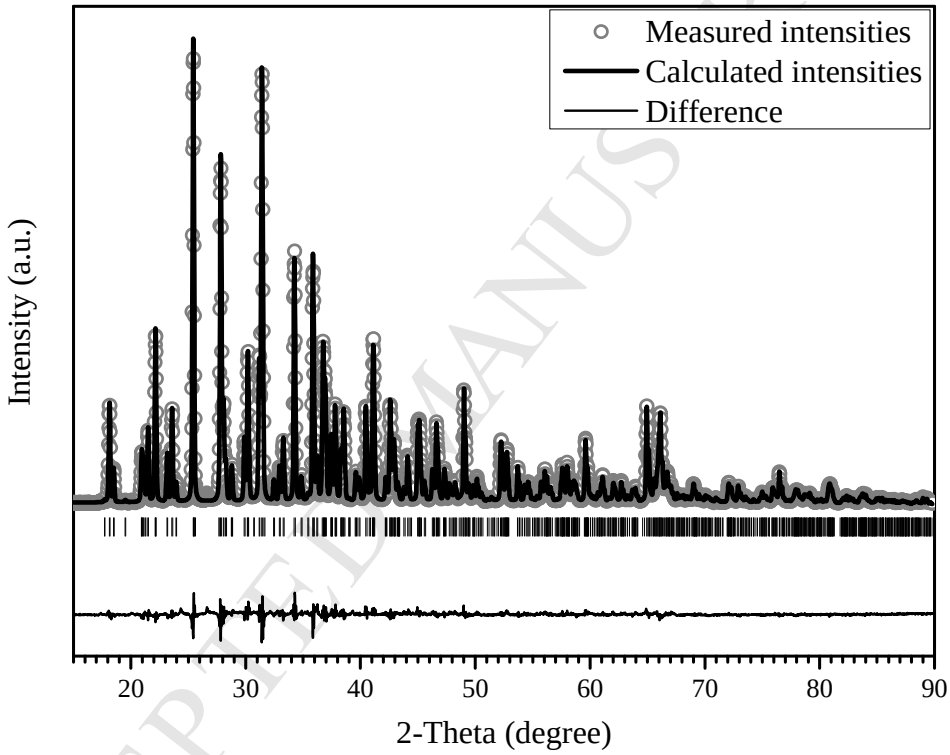

Figure 1. X-ray diffraction pattern of $Sr_4Al_{14}O_{25}$ refined employing Rietveld method. Sample prepared using H_3BO_3 (2.5% wt.) as a fluxing agent. Vertical bars located just below the background level indicate calculated positions of Bragg peaks for λ = 1.54059 Å (Cu Kα_1). (Figures of merit: R_p= 5.75%, R_{wp}= 7.46%, R_{exp}= 3.96%, χ^2= 3.55)

3.2. Partial substitution of Sr^{2+} by Ca^{2+}

To investigate the influence of partial substitution of strontium by calcium on the lattice parameters of $Sr_4Al_{14}O_{25}$, a series of samples $Sr_{(4-x)}Ca_xAl_{14}O_{25}$ x = 0, 0.05, 0.1, 0.2, 0.3, 0.5, 0.7, 1.0, 1.2, 1.4,

1.6, 1.8, 2.0 and 2.2 were prepared. From XRD data (representative patterns are given in Figure 2) it is visible that single phase compounds can be obtained with substitution up to x = 1.4. With higher substitutional level of Ca the secondary phase of $CaAl_4O_7$ is forming.

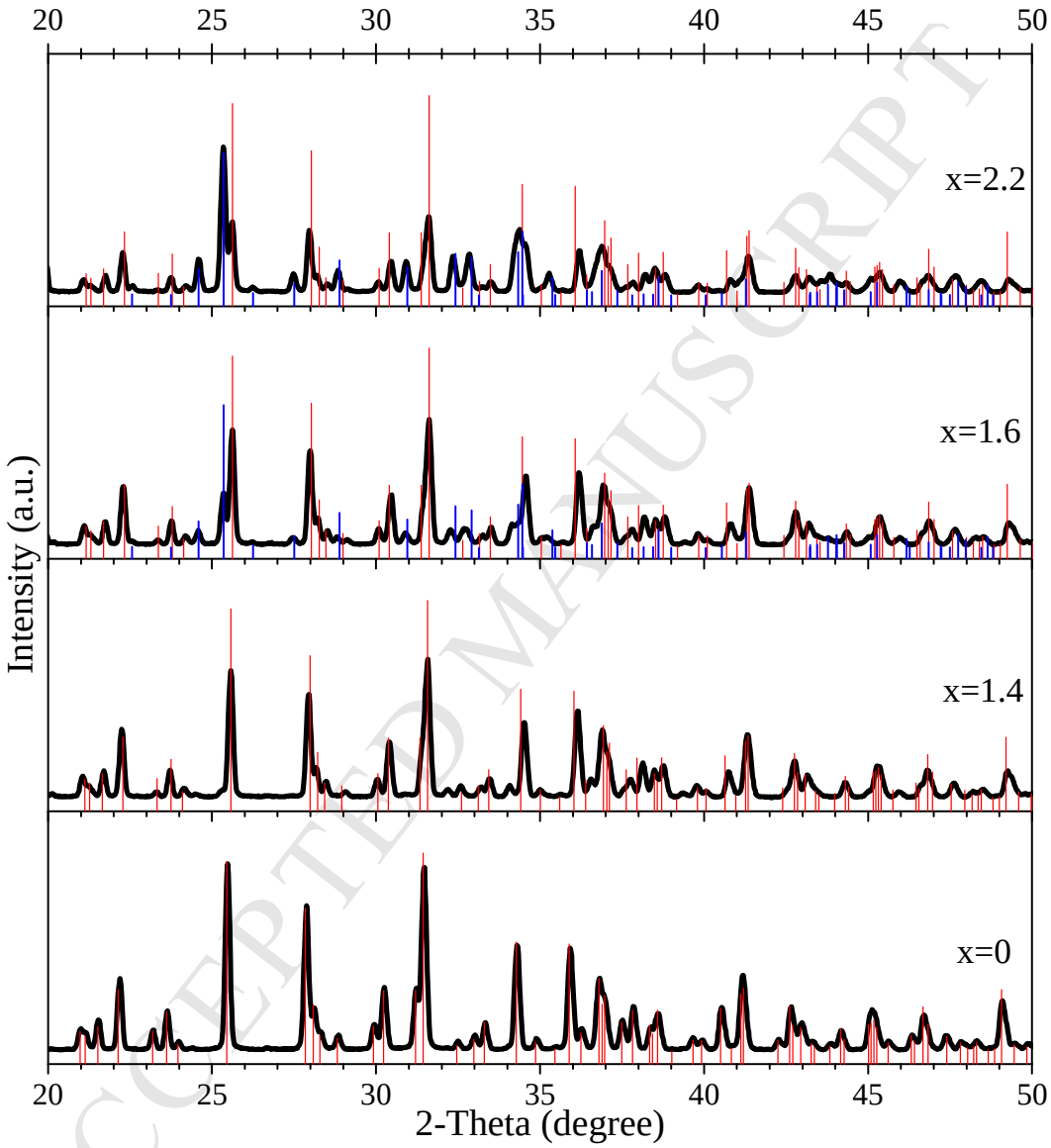

Figure 2. XRD patterns of $Sr_{(4-x)}Ca_xAl_{14}O_{25}$ samples. Red bars indicate standard pattern of $Sr_4Al_{14}O_{25}$ (PDF#00-074-1810) phase. Additional phase of $CaAl_4O_7$ (PDF#96-901-4426) is marked by blue bars.

These data are in a good agreement with published by Suriyamurthy et al. [30]. It was reported, that when calcium amount in $Sr_{(4-x)}Ca_xAl_{14}O_{25}$ samples was x = 3.2 the $Sr_4Al_{14}O_{25}$ phase was barely detectable and $CaAl_4O_7$ phase was dominant in the synthesis product.

Previously refined $Sr_4Al_{14}O_{25}$ data were used as a starting model for Rietveld refinement. The Ca^{2+} ions were assumed to occupy the Sr1 (4*j*) and Sr2 (4*i*) sites in the refinements and the sum of the Sr and Ca occupancies of these two sites were constrained to 0.5. Crystallographic data of $CaAl_4O_7$ (ICDS#14270) were used for the refinement when second phase was present in the samples (x >1.4). Refined lattice parameters *a*, *b* and *c* are shown in Figure 3. The crystallographic details of one selected representative sample (where x=1.4) refined from X-ray powder diffraction data are provided in Table 1.

Table 1. Structural parameters[a] for $Sr_{2.6}Ca_{1.4}Al_{14}O_{25}$[b] refined from X-ray powder diffraction data collected at room temperature using orthorhombic space group Pmma (No. 51).

Atom	x	y	z	B_{iso}	Occupancy	Site/ Multiplicity
Sr1	0.13790 (7)	1/2	0.03242 (50)	0.397 (65)	0.405 (4)	4*j*
Ca1	0.13790 (7)	1/2	0.03242 (50)	0.397 (65)	0.095 (4)	4*j*
Sr2	0.11965 (10)	0	0.12039 (64)	0.397 (65)	0.239 (4)	4*i*
Ca2	0.11965 (10)	0	0.12039 (64)	0.397 (65)	0.261 (4)	4*i*
Al1	0.18554 (16)	0.19266 (50)	0.62811 (100)	0.492 (58)	1	8*l*
Al2	0.06647 (16)	0.31970 (58)	0.51039 (106)	0.492 (58)	1	8*l*
Al3	1/4	0.29316 (68)	0.12979 (144)	0.492 (58)	1/2	4*k*
Al4	0	0.16716 (52)	0	0.492 (58)	1/2	4*g*
Al5	0	0	1/2	0.492 (58)	1/4	2*c*
Al6	0	1/2	0	0.492 (58)	1/4	2*e*
O1	0.04498 (28)	0.16206 (95)	0.31940 (208)	0.078 (82)	1	8*l*
O2	0.13781 (30)	0.31851 (84)	0.50152 (173)	0.078 (82)	1	8*l*
O3	0.18909 (27)	0.22533 (82)	-0.01895 (151)	0.078 (82)	1	8*l*
O4	1/4	0.23081 (122)	0.47781 (204)	0.078 (82)	1/2	4*k*
O5	0.04024 (43)	0	0.83537 (264)	0.078 (82)	1/2	4*i*
O6	0.05041 (40)	1/2	0.33651 (277)	0.078 (82)	1/2	4*j*
O7	0.16456 (39)	0	0.56937 (233)	0.078 (82)	1/2	4*i*
O8	0.04274 (26)	0.32899 (93)	0.85792 (219)	0.078 (82)	1	8*l*
O9	1/4	1/2	0.10010	0.078 (82)	1/4	2*f*

[a]: Numbers in parentheses are standard deviations of last significant digits. Values with no standard deviation shown were not refined.

[b]: Cell parameters: a= 24.57249 (34), b= 8.45725 (12), c= 4.86924 (7); Figures of merit: R_p= 9.26%, R_{wp}= 13.3%, R_{exp}= 4.58%, χ^2= 8.48.

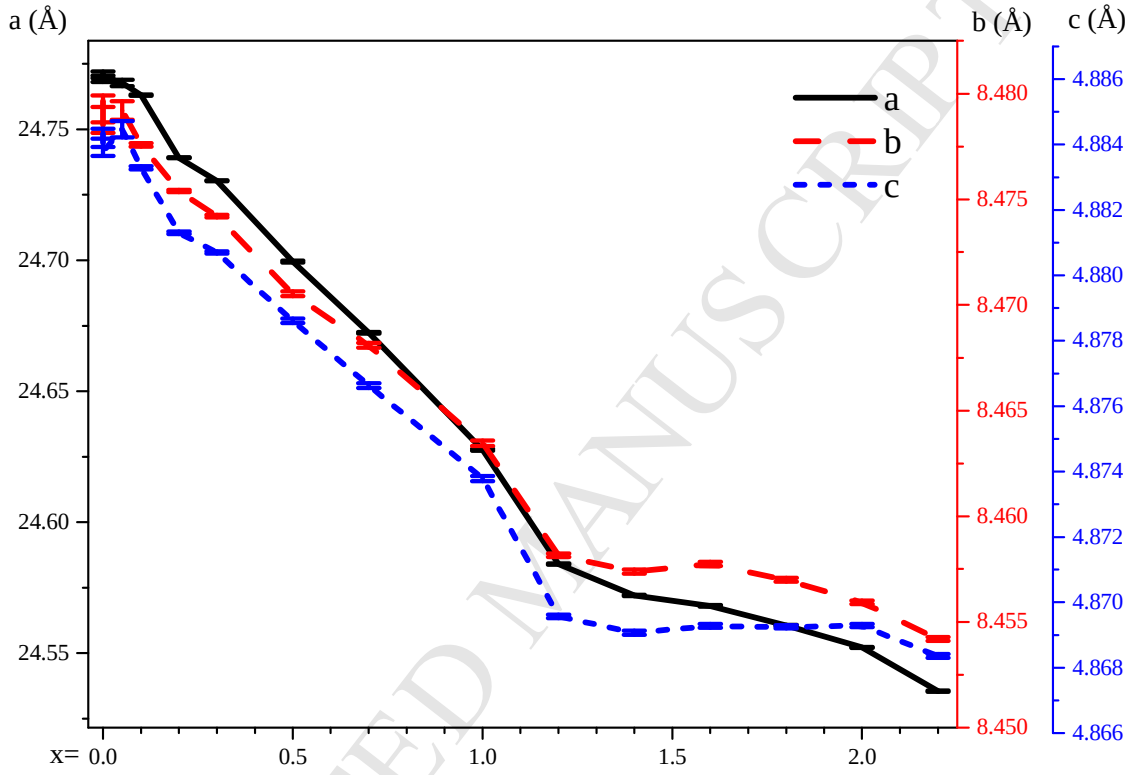

Figure 3. Refined lattice parameters *a*, *b* and *c* for $Sr_{(4-x)}Ca_xAl_{14}O_{25}$ plotted as a function Ca^{2+} doping level x.

As expected, substituting Sr^{2+} with Ca^{2+} (ionic radii 118 and 100 pm [41], respectively) caused unit cell volume and lattice parameters to shrink. The rate of change of all three lattice parameters *a*, *b* and *c* is seen to abruptly decrease when x reaches a value of approximately 1.3 which is close to the critical Ca^{2+} concentration x = 1.4 which is the upper limit for formation of single phase samples. The refined Ca occupancies of the Sr1 and Sr2 sites are plotted in Figure 4.

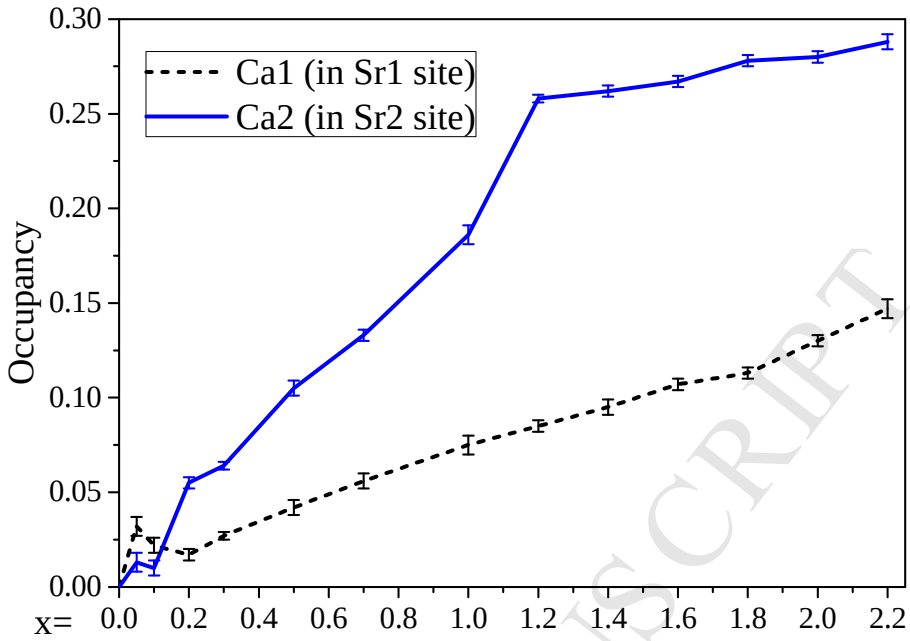

Figure 4. Refined occupancy parameters for two strontium sites in $Sr_{4-x}Ca_xAl_{14}O_{25}$ samples plotted as a function Ca^{2+} doping level x.

Except for the lowest calcium concentrations, the Sr2 site is more likely to be substituted by calcium. Furthermore, the rate of Ca substitution in the Sr2 site is seen to decrease for x > 1.2 which again reflects the onset of second phase formation. Figure 5 Shows the $Sr_4Al_{14}O_{25}$ crystal structure. The Sr1 sites are surrounded by AlO_4-tetrahedra while the Sr2 sites are surrounded by both AlO_4-tetrahedra and AlO_6-octahedra. The Sr2 sites (coordination number 7, average Sr2-O distance 2.636 Å) are more susceptible for Ca substitution as sites are less spacious than Sr1 sites (coordination number 10, average Sr1-O distance 2.811 Å).

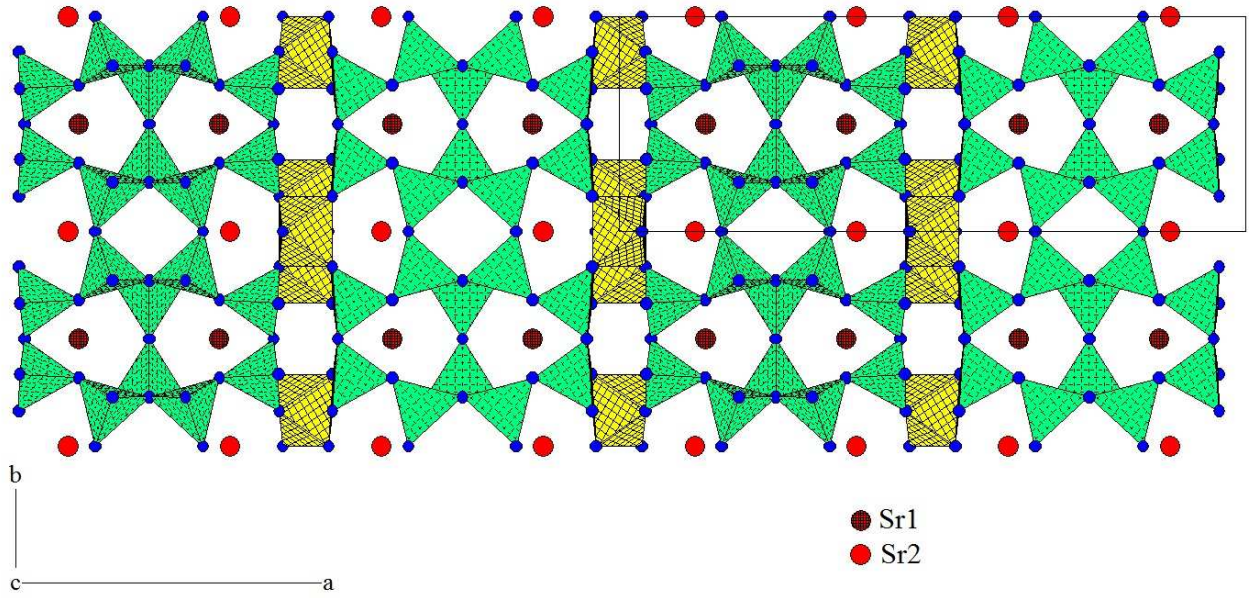

Figure 5. Projection of $Sr_4Al_{14}O_{25}$ crystal structure viewed along c-axis. Sr1 (red circles with squared patterns), Sr2 (red circles), AlO_4-tetrahedra (green) and AlO_6-octahedra (yellow).

3.3. Synthesis of Ce-doped $Sr_4Al_{14}O_{25}$

Cerium-doped $Sr_{4-y}Al_{14}O_{25}:Ce_y$ samples were prepared using the same synthetic approach and phase analysis of synthesis products was also performed**.** As seen from the XRD patterns presented in Figure 6, two compounds with the largest amount of cerium contain additionally traces of ceria (cerium(IV) oxide).

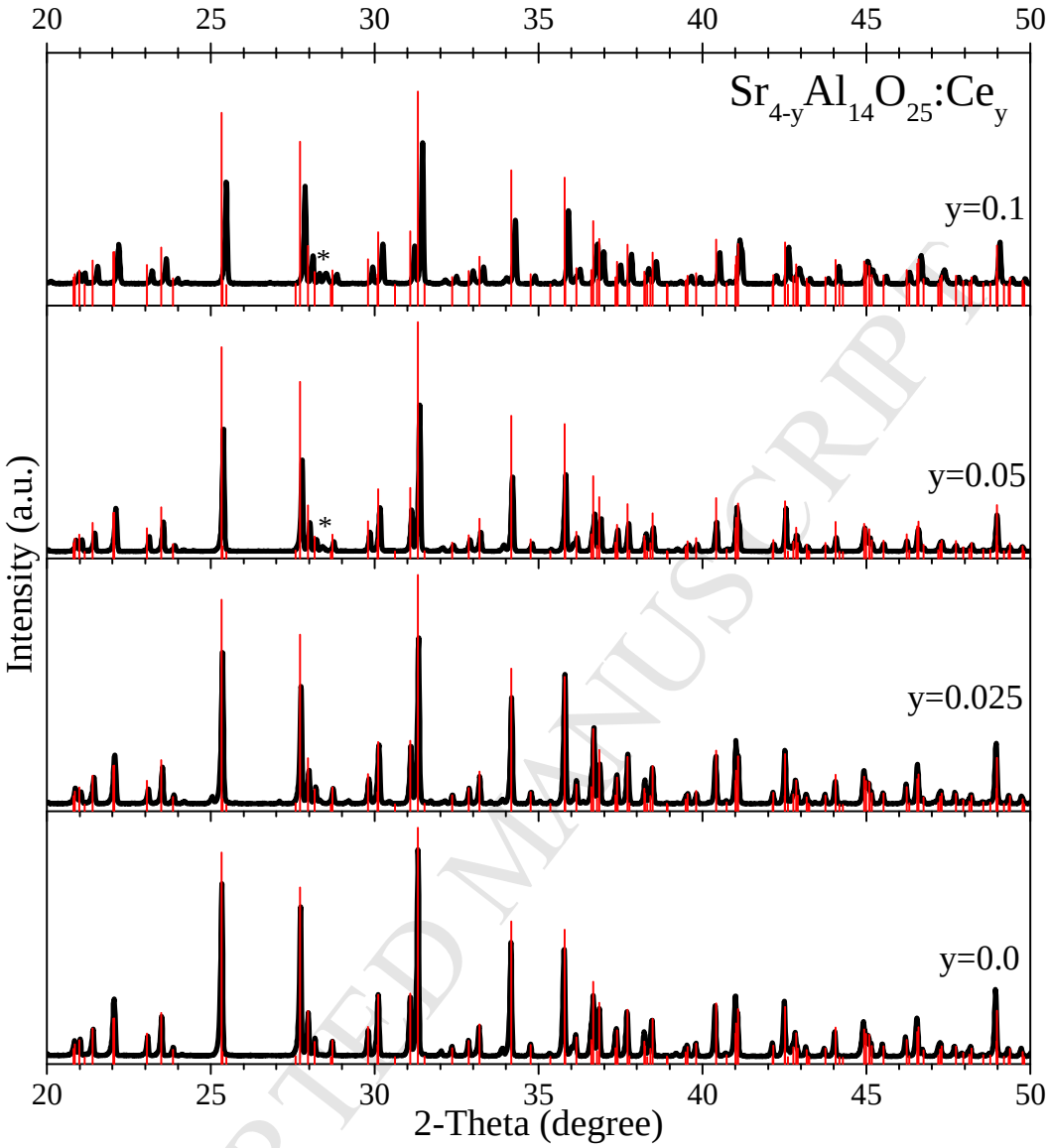

Figure 6. XRD patterns of $Sr_{4-y}Al_{14}O_{25}:Ce_y$. Red bars indicate standard pattern of $Sr_4Al_{14}O_{25}$ (PDF#00-074-1810) phase. The impurity phase is marked: * – CeO_2.

The Rietveld refinement for these samples was performed as well. The results obtained from the refinement imply that the amount of CeO_2 (the crystallographic data were obtained from COD – crystallographic open database, #4343161) present in the compounds are 1 % and 0.4 % for y = 0.1 and y = 0.05 accordingly. These results clearly show that even CeO_2 phase is forming as impurity, the largest part of cerium is still embedded into the structure of $Sr_{4-y}Al_{14}O_{25}:Ce_y$ (e.g. when y = 0.05, the total mol % of cerium is 1.25, so at least 0.75 mol % should be incorporated in the

structure). Attempts to refine the Ce occupancies Sr1 and Sr2 sites following the procedure used for Ca-doping were unsuccessful.

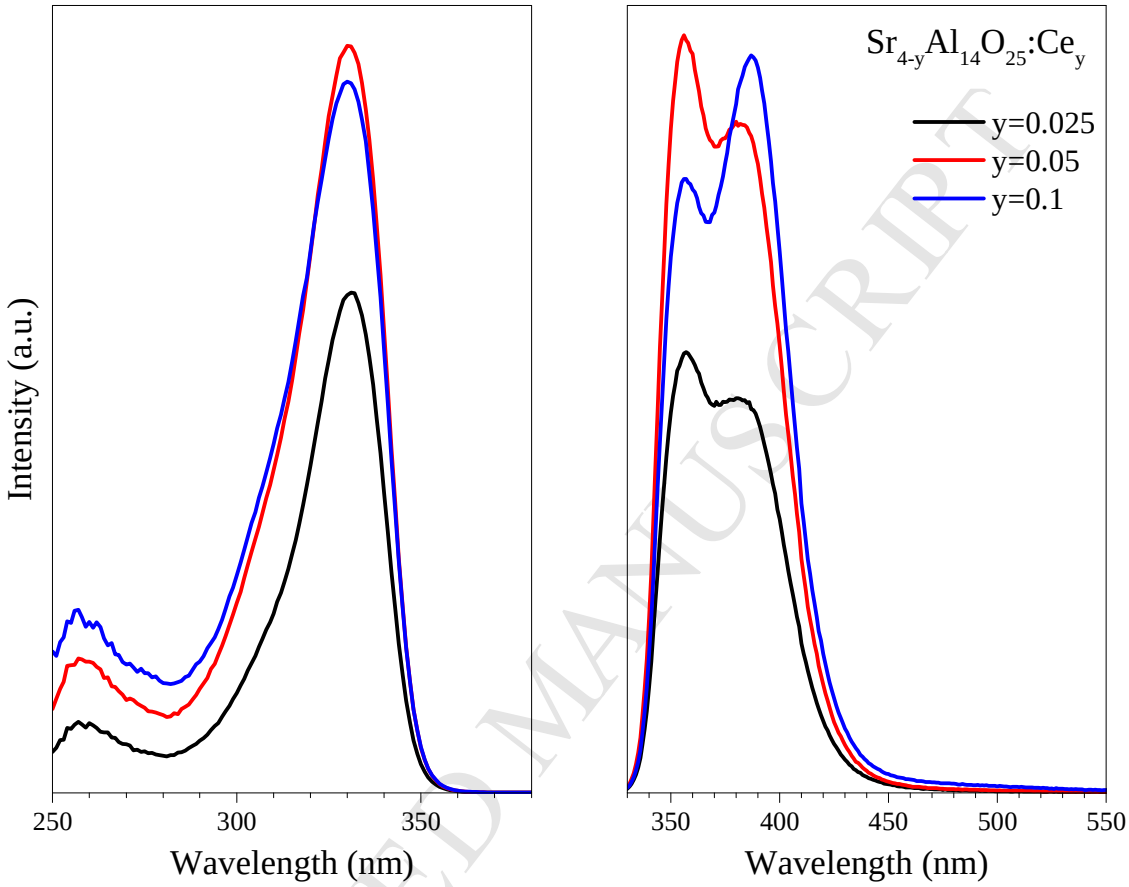

Figure 7. Excitation (λ_{em} = 360) at left and emission (λ_{ex} = 330 nm) at right spectra of $Sr_{4-y}Al_{14}O_{25}:Ce_y^{3+}$ samples.

Excitation and emission spectra of the $Sr_{4-y}Al_{14}O_{25}:Ce_y$ samples were also measured and are presented in Figure 7. Two emission maximums can be noticed: the first around 360 nm and the second around 380 nm, the excitation maximum is around 330 nm. The emission peaks are broad, this is due to the transition in Ce^{3+} ions from [Xe]$4d^1$ to [Xe]$5f^1$. As it can be seen from the spectra in Figure 7 the sample with y = 0.05 has the highest emission intensity. Higher level of doping results in decrease of intensity due to concentration quenching. Therefore, the doping with y = 0.05 was chosen for further investigations.

3.4. Partial substitution of Sr^{2+} by Ca^{2+} in cerium-doped samples

Cerium-doped strontium aluminates where strontium was partially substituted by calcium were synthesized to investigate the effects on the structural changes of the $Sr_{3.95}Al_{14}O_{25}:Ce_{0.05}$. A series of $Sr_{3.95-x}Ca_xAl_{14}O_{25}:Ce_{0.05}$ samples where x=0.1, 0.4, 0.6, 0.8, 1.0, 1.2 and 1.4 were prepared using the same synthesis method. XRD data of the representative compounds are shown in Figure 8.

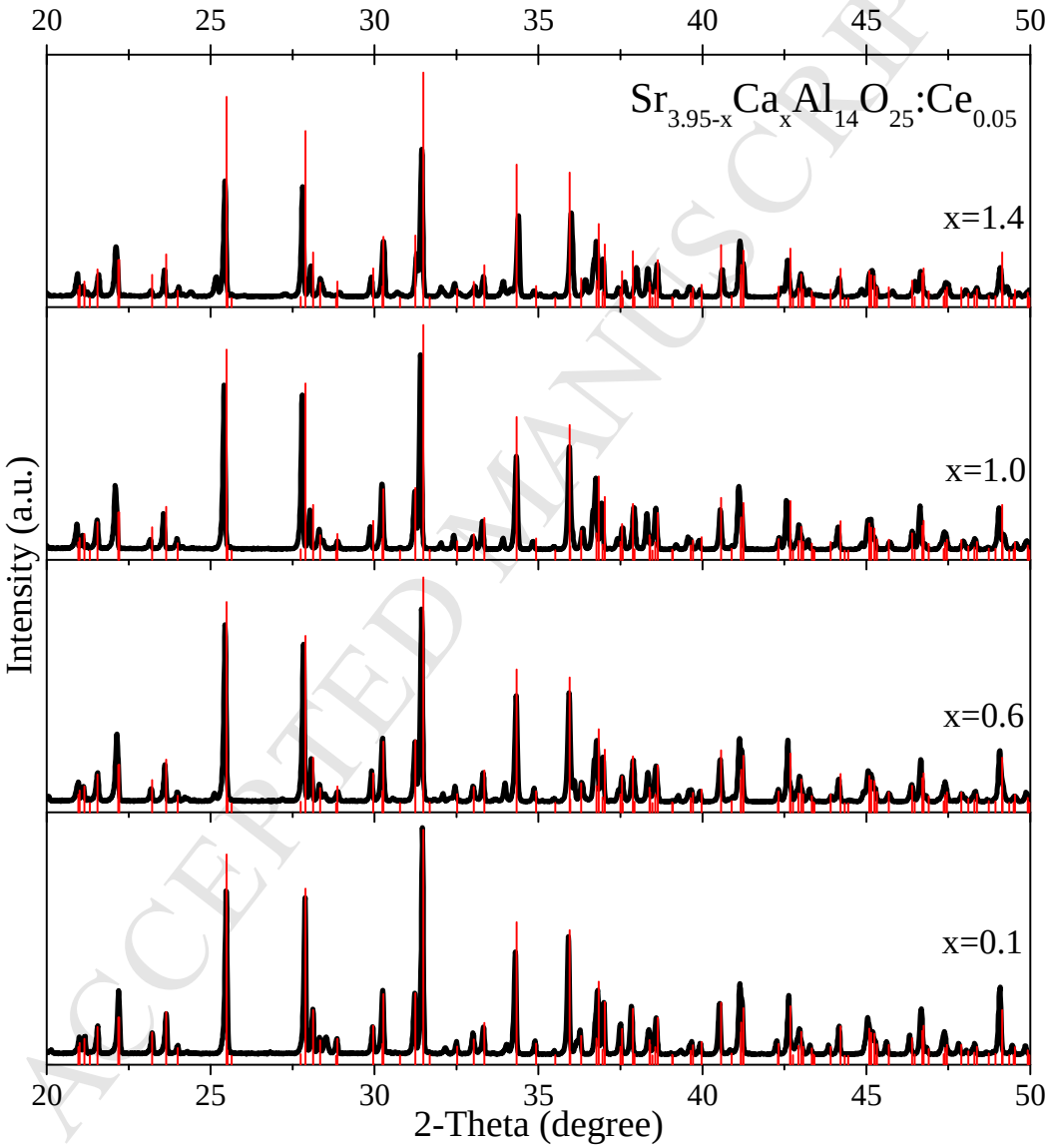

Figure 8. XRD patterns of $Sr_{3.95-x}Ca_xAl_{14}O_{25}:Ce_{0.05}$. Red bars indicate standard pattern of $Sr_4Al_{14}O_{25}$ (PDF#00-074-1810) phase.

All compounds from the synthesized series were refined using the Rietveld method. The result of $Sr_{3.95}Al_{14}O_{25}:Ce_{0.05}$ refinement which was performed earlier was used as basis for this series

refinement. The refinement results for cell parameters and their dependence are depicted in Figure 9. As in undoped samples described previously, all cell parameters are decreasing linearly with increasing the level of Sr^{2+} substitution by Ca^{2+}.

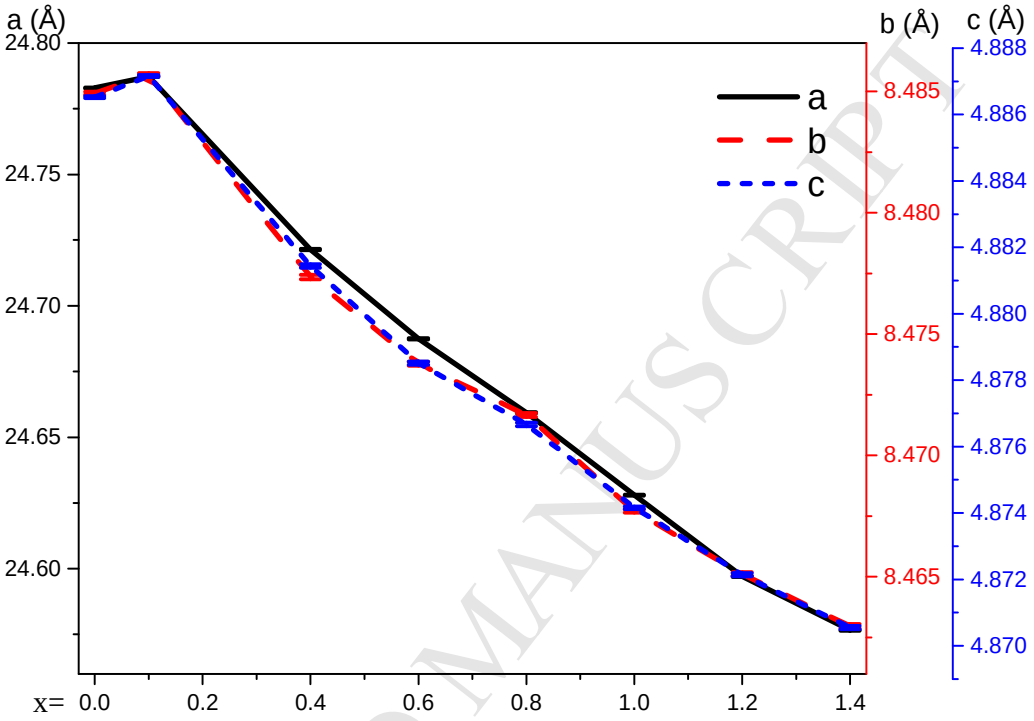

Figure 9. Refined lattice parameters *a*, *b* and *c* for $Sr_{3.95-x}Ca_xAl_{14}O_{25}:Ce_{0.05}$ plotted as a function Ca^{2+} doping level x.

Occupation factors were refined by introducing the constraints as explained previously (Sr1 + Ca1 = 0.5, Sr2 + Ca2 = 0.5). Once again, both Ca1 and Ca2 occupancies are increasing linearly when substitution level is increased. Also it can be seen that Sr2 is a much more preferred site for calcium, and except for the smallest amounts it was at least 3-4 times more substituted by calcium.

Excitation and emission spectra of photoluminescence measurements are presented in Figure 10. The decrease of excitation and emission intensities was observed by substituting even small amount of Sr by Ca, however, at higher levels of substitution the intensities of emission monotonically increase. Unsubstituted sample falls around the middle of our range of substitution and its

integrated intensity is close to that of the $Sr_{3.35}Ca_{0.6}Al_{14}O_{25}:Ce_{0.05}$ sample (see inset of Figure 10). The highest intensity was determined for the most substituted aluminate (x = 1.4).

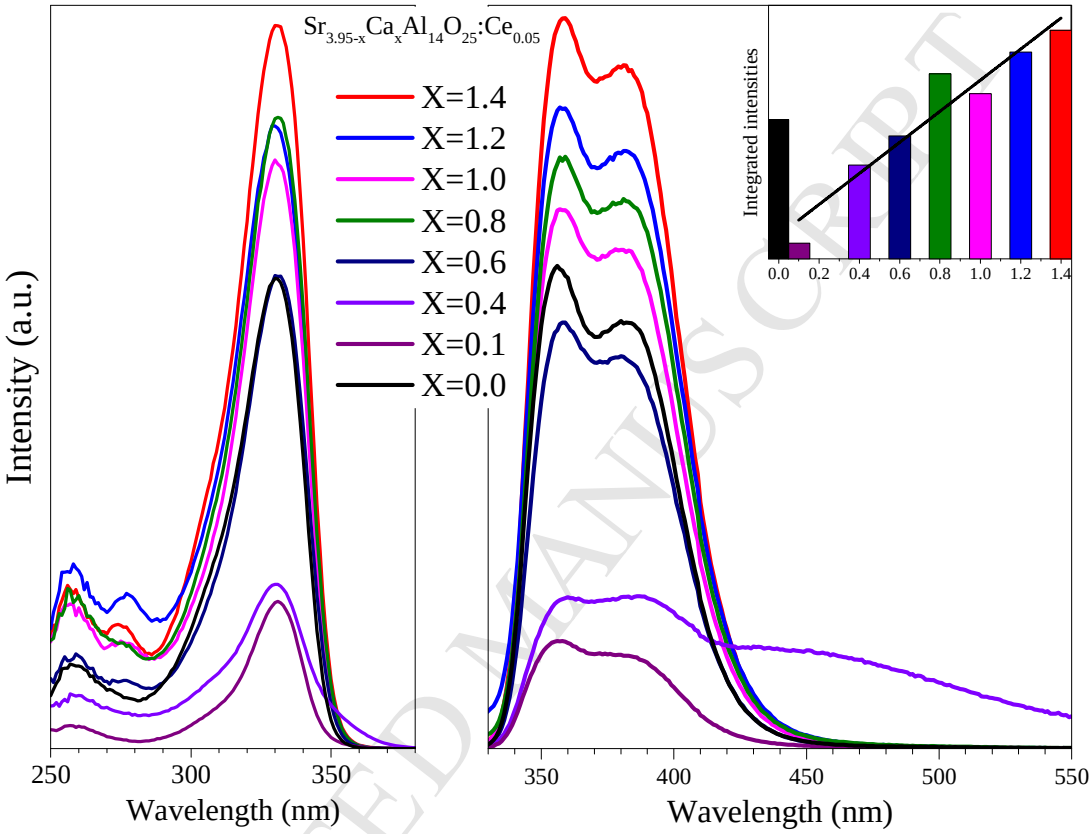

Figure 10. Excitation (λ_{em} = 360 nm) at left and emission (λ_{ex} = 330 nm) at right spectra of $Sr_{3.95-x}Ca_xAl_{14}O_{25}:Ce_{0.05}$ samples. Figure inset – integrated emission intensities plotted as a function Ca^{2+} doping level x.

Quantum yields and luminescence kinetics for the synthesized samples were also measured. Decay curves are presented in Figure 11. Decay constants of monoexponential fits are presented in Table 2 along with quantum yield calculation results and positions of emission peak maximums. Both, quantum yields and decay times, slightly increase with increasing amount of Ca while unsubstituted sample is in the middle of the range.

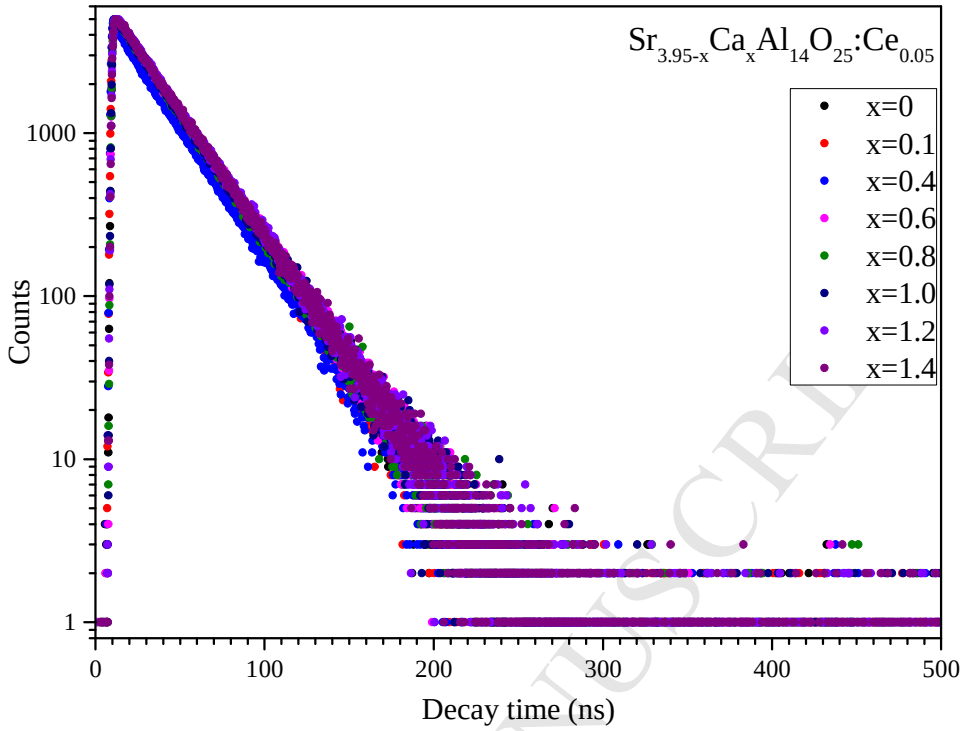

Figure 11. Decay curves for $Sr_{3.95-x}Ca_xAl_{14}O_{25}:Ce_{0.05}$ samples. (λ_{ex} = 330 nm, λ_{em} = 360 nm)

Table 2. Emission maximums, quantum yields and τ_1 constant determined for $Sr_{3.95-x}Ca_xAl_{14}O_{25}:Ce_{0.05}$ samples (numbers in parenthesis note the deviation of last significant digit).

x=	0.0	0.1	0.4	0.6	0.8	1.0	1.2	1.4
Ca amount (%)	0	2.5	10	15	20	25	30	35
λem maximum (nm)	356	357	360	359	359	359	359	359
Quantum yield (%)	16.93	6.16	10.63	16.86	22.42	22.88	22.26	27.11
τ1 (1/ns)	27.87 (4)	27.56 (4)	27.54 (5)	28.11 (4)	28.34 (4)	28.17 (4)	28.35 (4)	28.39 (4)

4. Conclusions

It was demonstrated that partial substitution of calcium for strontium in $Sr_{4-x}Ca_xAl_{14}O_{25}$ is possible up to x=1.4 obtaining monophasic samples, while higher concentrations of Ca result in occurrence of additional phases. Refinement of crystal structures showed that such substitution results in

shrinkage of unit cell parameters due to smaller radius of Ca^{2+} ion. Moreover, cerium-doped samples $Sr_{4-y}Al_{14}O_{25}:Ce_y^{3+}$ and $Sr_{3.95-x}Ca_xAl_{14}O_{25}:Ce_{0.05}$ were prepared as well. The luminescent and structural properties of these samples were investigated. Refinement of site occupancy parameters revealed that Sr2 site (of two strontium sites in the crystal structure) is more likely to be substituted by the smaller calcium ion, however, the site preference of cerium could not be reliably determined using X-ray diffraction analysis. Evidently, further investigation on cerium substitutional effects should be performed in future. Examination of luminescence properties showed that the $Sr_4Al_{14}O_{25}:Ce_y^{3+}$ sample with y = 0.05 showed the highest emission intensity. In overall, for the $Sr_{3.95-x}Ca_xAl_{14}O_{25}:Ce_{0.05}$ samples all measured properties (excitation and emission intensities, decay times and quantum yields) increased with increasing substitutional level of calcium. However, the values of unsubstituted sample were close to the middle of the range of substituted samples.

Acknowledgement

This research is funded by the European Social Fund under the No 09.3.3-LMT-K-712 "Development of Competences of Scientists, other Researchers and Students through Practical Research Activities" measure.

References

1. Gunay, B.E.a.V., *Effects of La_2O_3 addition on the thermal stability of g-Al_2O_3 gels.* Ceramics International, 30 (2004), p.p. 163-170. DOI: 10.1016/S0272-8842(03)00084-1.
2. Katelnikovas A., B.T., Vitta P., Justel T., Winkler H., Kareiva A., Zukauskas A. and Tamulaitis G., *$Y_{3-x}Mg_2AlSi_2O_{12}:Ce_x^{3+}$ phosphors - prospective for warm-white light emitting diodes.* Optical Materials, 32 (2010), p.p. 1261-1265. DOI: 10.1016/j.optmat.2010.04.031.
3. Sun, T.X., *Combinatorial search for advanced luminescence materials.* Biotechnology and Bioengineering, 61 (1999), p.p. 193-201. DOI: 10.1002/(SICI)1097-0290(1998)61:4%3C193::AID-CC2%3E3.0.CO;2-8.
4. Toncelli, A., A. Di Lieto, P. Minguzzi, and M. Tonelli, *Discovering energy-transfer paths in laser materials.* Optics letters, 22 (1997), p.p. 1165-1167. DOI: 10.1364/OL.22.001165.
5. Douy, A. and M. Capron, *Crystallisation of spray-dried amorphous precursors in the SrO–Al_2O_3 system: a DSC study.* Journal of the European Ceramic Society, 23 (2003), p.p. 2075-2081. DOI: 10.1016/s0955-2219(03)00015-3.
6. Haranath, D., V. Shanker, H. Chander, and P. Sharma, *Tuning of emission colours in strontium aluminate long persisting phosphor.* Journal of Physics D-Applied Physics, 36 (2003), p.p. 2244-2248. DOI: 10.1088/0022-3727/36/18/012.

7. Avdeev, M., S. Yakovlev, A.A. Yaremchenko, and V.V. Kharton, *Transitions between $P2_1$, $P6_3$, and $P6_322$ modifications of $SrAl_2O_4$ by in situ high-temperature X-ray and neutron diffraction.* Journal of Solid State Chemistry, 180 (2007), p.p. 3535-3544. DOI: 10.1016/j.jssc.2007.10.021.
8. Lin, Y.H., Z.L. Tang, Z.T. Zhang, and C.W. Nan, *Anomalous luminescence in Sr4Al14O25 : Eu, dy phosphors.* Applied Physics Letters, 81 (2002), p.p. 996-998. DOI: 10.1063/1.1490631.
9. Lin, Y.H., Z.L. Tang, and Z.T. Zhang, *Preparation of long-afterglow $Sr_4Al_{14}O_{25}$-based luminescent material and its optical properties.* Materials Letters, 51 (2001), p.p. 14-18. DOI: 10.1016/S0167-577x(01)00257-9.
10. Sharma, S.K., S.S. Pitale, M.M. Malik, R.N. Dubey, and M.S. Qureshi, *Synthesis and detailed kinetic analysis of $Sr_4Al_{14}O_{25}:Eu^{2+}$ phosphor under black light irradiation.* Radiation Effects and Defects in Solids, 163 (2008), p.p. 767-777. DOI: 10.1080/10420150701772984.
11. Nakazawa, E., Y. Murazaki, and S. Saito, *Mechanism of the persistent phosphorescence in Sr4Al14O25 : Eu and SrAl2O4 : Eu codoped with rare earth ions.* Journal of Applied Physics, 100 (2006), p.p. 113113. DOI: 10.1063/1.2397284.
12. Zhong, R.X., J.H. Zhang, X. Zhang, S.Z. Lu, and X.J. Wang, *Red phosphorescence in Sr4Al14O25 : Cr3+,Eu2+,Dy3+ through persistent energy transfer.* Applied Physics Letters, 88 (2006), p.p. 201916. DOI: 10.1063/1.2205167.
13. Chen, L., Y. Zhang, F. Liu, W. Zhang, X. Deng, S. Xue, A. Luo, Y. Jiang, and S. Chen, *The red luminescence of $Sr_4Al_{14}O_{25}:Mn^{4+}$ enhanced by coupling with the $SrAl_2O_4$ phase in the $3SrO \cdot 5Al_2O_3$ system.* physica status solidi (a), 210 (2013), p.p. 1791-1796. DOI: 10.1002/pssa.201329108.
14. Sakirzanovas, S., A. Katelnikovas, D. Dutczak, A. Kareiva, and T. Justel, *Synthesis and Sm^{2+}/Sm^{3+} doping effects on photoluminescence properties of $Sr_4Al_{14}O_{25}$.* Journal of Luminescence, 131 (2011), p.p. 2255-2262. DOI: 10.1016/j.jlumin.2011.05.060.
15. Luitel, H.N., T. Watari, R. Chand, T. Torikai, and M. Yada, *Photoluminescence properties of a novel orange red emitting $Sr_4Al_{14}O_{25}:Sm^{3+}$ phosphor and PL enhancement by Bi^{3+} co-doping.* Optical Materials, 34 (2012), p.p. 1375-1380. DOI: 10.1016/j.optmat.2012.02.025.
16. Manashirov, O.Y., E.M. Zvereva, V.B. Gutan, A.N. Gorgobiani, S.A. Ambrozevich, and A.N. Lobanov, *A new photostimulated strontium-aluminate-based blue-green phosphor.* Inorganic Materials, 49 (2013), p.p. 487-491. DOI: 10.1134/S0020168513040080.
17. Han, S.H. and Y.J. Kim, *Luminescent properties of ce and eu doped Sr4Al14O25 phosphors.* Optical Materials, 28 (2006), p.p. 626-630. DOI: 10.1016/j.optmat.2005.09.031.
18. Sharma, S.K., S.S. Pitale, M. Manzar Malik, R.N. Dubey, and M.S. Qureshi, *Luminescence studies on the blue–green emitting $Sr_4Al_{14}O_{25}:Ce^{3+}$ phosphor synthesized through solution combustion route.* Journal of Luminescence, 129 (2009), p.p. 140-147. DOI: 10.1016/j.jlumin.2008.09.002.
19. Nikhare, G.N., S.C. Gedam, and S.J. Dhoble, *Luminescence in Sr4 Al14 O25 :Ce(3+) aluminate phosphor.* Luminescence, 30 (2015), p.p. 163-7. DOI: 10.1002/bio.2708.
20. Akiyama, M., C. Xu, H. Matsui, K. Nonaka, and T. Watanabe, *Photostimulated luminescence phenomenon of Sr4AI14O25 : Eu,Dy using only visible lights.* JOURNAL OF MATERIALS SCIENCE LETTERS, 19 (2000), p.p. 1163 - 1165. DOI: 10.1023/A:1006763310775.
21. Suriyamurthy, N. and B.S. Panigrahi, *Luminescence studies during combustion synthesis of a long afterglow phosphor Sr4Al14O25:Eu2+, Dy3+.* Indian Journal of Engineering and Materials Sciences, 16 (2009), p.p. 178-180. DOI: http://nopr.niscair.res.in/handle/123456789/4780.

22. Sharma, S., S. Pitale, M.M. Malik, R.N. Dubey, M.S. Qureshi, S.K. Vasisth, and P. Pathak, *Synthesis and thermoluminescence studies of Sr4Al14O25:Eu2+ phosphor.* Indian Journal of Engineering and Materials Sciences, 16 (2009), p.p. 165-168. DOI: http://nopr.niscair.res.in/handle/123456789/4790.
23. Liu, W.-R., C.C. Lin, Y.-C. Chiu, Y.-T. Yeh, S.-M. Jang, and R.-S. Liu, *Luminescence Properties of Green-emitting Phosphors-Sr4Al14O25:Eu2+ for LED Applications.* Journal of Chemistry and Chemical Engineering, 5 (2011), p.p. 638-643.
24. Chang, C.-C., C.-Y. Yang, and C.-H. Lu, *Preparation and photoluminescence properties of Sr4Al14O25:Eu2+ phosphors synthesized via the microemulsion route.* Journal of Materials Science: Materials in Electronics, 24 (2012), p.p. 1458-1462. DOI: 10.1007/s10854-012-0952-x.
25. Dacyl, D., D. Uhlich, and T. Justel, *The effect of calcium substitution on the afterglow of Eu2+/Dy3+ doped Sr4Al14O25.* Central European Journal of Chemistry, 7 (2009), p.p. 164-167. DOI: 10.2478/s11532-009-0017-z.
26. Li, Q., J.W. Zhao, and F.L. Sun, *Energy transfer mechanism of Sr4Al14O25:Eu2+ phosphor.* Journal of Rare Earths, 28 (2010), p.p. 26-29. DOI: 10.1016/S1002-0721(09)60043-0.
27. Luitel, H.N., T. Watari, T. Torikai, and M. Yada, *Effects of Particle Size and Type of Alumina on the Morphology and Photoluminescence Properties of Sr4Al14O25:Eu2+/Dy3+ Phosphor.* Research Letters in Materials Science, 2009 (2009), p.p. 1-4. DOI: 10.1155/2009/475074.
28. Luitel, H.N., T. Watari, T. Torikai, M. Yada, R. Chand, C.N. Xu, and K. Nanoka, *Highly water resistant surface coating by fluoride on long persistent Sr4Al14O25:Eu2+/Dy3+ phosphor.* Applied Surface Science, 256 (2010), p.p. 2347-2352. DOI: 10.1016/j.apsusc.2009.10.065.
29. Mishra, S.B., A.K. Mishra, A.S. Luyt, N. Revaprasadu, K.T. Hillie, W.J.V. Steyn, E. Coetsee, and H.C. Swart, *Ethyl Vinyl Acetate Copolymer-SrAl2O4:Eu,Dy and Sr4Al14O25:Eu,Dy Phosphor-Based Composites: Preparation and Material Properties.* Journal of Applied Polymer Science, 115 (2010), p.p. 579-587. DOI: 10.1002/app.30976.
30. Suriyamurthy, N. and B.S. Panigrahi, *Effects of non-stoichiometry and substitution on photoluminescence and afterglow luminescence of Sr4Al14O25 : Eu2+, Dy3+ phosphor.* Journal of Luminescence, 128 (2008), p.p. 1809-1814. DOI: 10.1016/j.jlumin.2008.05.001.
31. Wu, Z., J. Shi, J. Wang, M. Gong, and Q. Su, *Synthesis and luminescent properties of Sr4Al14O25:Eu2+ blue–green emitting phosphor for white light-emitting diodes (LEDs).* Journal of Materials Science: Materials in Electronics, 19 (2007), p.p. 339-342. DOI: 10.1007/s10854-007-9325-2.
32. Xie, W., Y.-H. Wang, C.-W. Zou, F. Liang, J. Quan, J. Zhang, and L.-X. Shao, *Effect of H3BO3on the phase stability and long persistence properties of Sr3.96Al14O25:Eu2+0.01, Dy3+0.02phosphor.* Chinese Physics B, 22 (2013), p.p. 056101. DOI: 10.1088/1674-1056/22/5/056101.
33. Zhao, C.L., D.H. Chen, Y.H. Yuan, and M. Wu, *Synthesis of Sr4Al14O25 : Eu2+,Dy3+ phosphor nanometer powders by combustion processes and its optical properties.* Materials Science and Engineering B-Solid State Materials for Advanced Technology, 133 (2006), p.p. 200-204. DOI: 10.1016/j.mseb.2006.06.042.
34. Wang, D., M. Wang, and G. Lü, *Synthesis, crystal structure and X-ray powder diffraction data of the phosphor matrix 4SrO·7Al2O3.* JOURNAL OF MATERIALS SCIENCE, 34 (1999), p.p. 4959-4964. DOI: 10.1023/A:1004759621850.
35. Capron, M., F. Fayon, D. Massiot, and A. Douy, *Sr4Al14O25: Formation, Stability, and 27Al High-Resolution NMR Characterization.* Chemistry of Materials, 15 (2003), p.p. 575-579. DOI: 10.1021/cm0213265.

36. Blasse, G. and B.C. Grabmaier, *Luminescent materials*. 1994, Berlin: Springer. 232.
37. Peng, M., X. Yin, P.A. Tanner, M.G. Brik, and P. Li, *Site Occupancy Preference, Enhancement Mechanism, and Thermal Resistance of Mn4+ Red Luminescence in Sr4Al14O25: Mn4+ for Warm WLEDs.* Chemistry of Materials, 27 (2015), p.p. 2938-2945. DOI: 10.1021/acs.chemmater.5b00226.
38. Van den Eeckhout, K., D. Poelman, and P.F. Smet, *Persistent Luminescence in Non-Eu(2+)-Doped Compounds: A Review.* Materials (Basel), 6 (2013), p.p. 2789-2818. DOI: 10.3390/ma6072789.
39. Rodríguez-Carvajal, J., *Recent advances in magnetic structure determination by neutron powder diffraction.* Physica B: Condensed Matter, 192 (1993), p.p. 55-69. DOI: 10.1016/0921-4526(93)90108-I.
40. Grigorjevaite, J. and A. Katelnikovas, *Luminescence and Luminescence Quenching of K2Bi(PO4)(MoO4):Eu(3+) Phosphors with Efficiencies Close to Unity.* ACS Appl Mater Interfaces, 8 (2016), p.p. 31772-31782. DOI: 10.1021/acsami.6b11766.
41. Shannon, R., *Revised effective ionic radii and systematic studies of interatomic distances in halides and chalcogenides.* Acta Crystallographica Section A, 32 (1976), p.p. 751-767. DOI: 10.1107/S0567739476001551.

List of figures:

Figure 1. X-ray diffraction pattern of $Sr_4Al_{14}O_{25}$ refined employing Rietveld method. Sample prepared using H_3BO_3 (2.5% wt.) as a fluxing agent. Vertical bars located just below the background level indicate calculated positions of Bragg peaks for λ = 1.54059 Å (Cu Kα_1). (Figures of merit: R_p= 5.75%, R_{wp}= 7.46%, R_{exp}= 3.96%, χ^2= 3.55)

Figure 2. XRD patterns of $Sr_{(4-x)}Ca_xAl_{14}O_{25}$ samples. Red bars indicate standard pattern of $Sr_4Al_{14}O_{25}$ (PDF#00-074-1810) phase. Additional phase of $CaAl_4O_7$ (PDF#96-901-4426) is marked by blue bars.

Figure 3. Refined lattice parameters *a*, *b* and *c* for $Sr_{(4-x)}Ca_xAl_{14}O_{25}$ plotted as a function Ca^{2+} doping level x.

Figure 4. Refined occupancy parameters for two strontium sites in $Sr_{4-x}Ca_xAl_{14}O_{25}$ samples plotted as a function Ca^{2+} doping level x.

Figure 5. Projection of $Sr_4Al_{14}O_{25}$ crystal structure viewed along c-axis. Sr1 (red circles with squared patterns), Sr2 (red circles), AlO_4-tetrahedra (green) and AlO_6-octahedra (yellow).

Figure 6. XRD patterns of $Sr_{4-y}Al_{14}O_{25}:Ce_y$. Red bars indicate standard pattern of $Sr_4Al_{14}O_{25}$ (PDF#00-074-1810) phase. The impurity phase is marked: * – CeO_2.

Figure 7. Excitation (λ_{em} = 360) at left and emission (λ_{ex} = 330 nm) at right spectra of $Sr_{4-y}Al_{14}O_{25}:Ce_y^{3+}$ samples.

Figure 8. XRD patterns of $Sr_{3.95-x}Ca_xAl_{14}O_{25}:Ce_{0.05}$. Red bars indicate standard pattern of $Sr_4Al_{14}O_{25}$ (PDF#00-074-1810) phase.

Figure 9. Refined lattice parameters *a*, *b* and *c* for $Sr_{3.95-x}Ca_xAl_{14}O_{25}:Ce_{0.05}$ plotted as a function Ca^{2+} doping level x.

Figure 10. Excitation (λ_{ex} = 330 nm) at left and emission (λ_{ex} = 360 nm) at right spectra of $Sr_{3.95-x}Ca_xAl_{14}O_{25}:Ce_{0.05}$ samples. Figure inset – integrated emission intensities plotted as a function Ca^{2+} doping level x.

Figure 11. Decay curves for $Sr_{3.95-x}Ca_xAl_{14}O_{25}:Ce_{0.05}$ samples. (λ_{ex} = 330 nm, λ_{em} = 360 nm)

Highlights:

- Monophasic pure and modified $Sr_4Al_{14}O_{25}$ samples were prepared
- Sr was partially substituted by Ca without change in phase composition
- Ce-doped $Sr_4Al_{14}O_{25}$ samples (unsubstituted and partially substituted) were prepared
- Effect of partial substitution on luminescence was studied